JOURNAL OF MATERIALS SCIENCE 32 (1997) 6489–6494

High temperature thermoelectric properties and figure-of-merit of sintered $Nd_{2-x}Ce_xCuO_4$

M. YASUKAWA*, N. MURAYAMA
National Industrial Research Institute of Nagoya, Hirate-cho, Kita-ku, Nagoya 462, Japan

Thermoelectric properties such as the Seebeck coefficient, electrical resistivity, and thermal conductivity are measured in the temperature range of 300–673 K on $Nd_{2-x}Ce_xCuO_4$ ($x=0$–0.1) sintered bodies in order to estimate the figure-of-merit for thermoelectric energy conversion. The temperature dependences of both the Seebeck coefficient and electrical resistivity indicated n-type semiconducting behaviour. The thermal conductivities whose value decreased with increasing temperature were in the range of 3.7–7.5 $Wm^{-1}K^{-1}$. The maxima of the power factor and the figure-of-merit estimated from data measured at 320 K on a sample of a composition of $x=0.05$ were 9.2×10^{-5} $Wm^{-1}K^{-2}$ and 1.7×10^{-5} K^{-1}, respectively. The limitation of the power factor is discussed based on the measured Seebeck coefficient and electrical conductivity data. The thermal conductivity could be separated into a small electron component and a large phonon component by applying the Wiedemann–Franz law. This suggests the possibility of improving the figure-of-merit to some extent by a reduction of the phonon thermal conductivity.

1. Introduction

Since the discovery of high-temperature superconducting cuprate (HTSC) in doped La_2CuO_4 numerous other doped cuprates have been shown to display this property. These cuprates generally have common features in that they are charge-transfer-type insulators without any doping, and change to normal metals with heavy doping [1]. In the lower doping region they show semiconducting behaviour with a relatively large Seebeck coefficient. Therefore, several investigations on the possibility of using HTSCs as thermoelectric energy conversion materials have been reported in the literature [2, 3]. The thermoelectric figure-of-merit (Z) can be expressed as:

$$Z = S^2\sigma/\lambda \quad (1)$$

where S, σ, and λ are the Seebeck coefficient, electrical conductivity, and thermal conductivity, respectively. Large values of the Seebeck coefficient and electrical conductivity, and a small thermal conductivity are required for a high value of the figure-of-merit. Mason [3] has reported the potential application of HTSCs in thermoelectric energy conversion. His arguments are based on the values of the Seebeck coefficient and the electrical conductivity that are measured as a function of the dopant concentration [3]. It has been suggested that HTSCs could operate as passive thermoelectric energy conversion materials, since the values of the power factor ($S^2\sigma$) are intrinsically small as compared to the values shown by band semiconductors such as Bi_2Te_3-based materials. It should be noted that the value of $S^2\sigma$ can be maximized by optimization of the carrier concentration. Currently there are few reports in the literature on the experimental estimation of the figure-of-merit and its temperature dependence for HTSCs, and it is the aim of this work to rectify this situation.

The combined use of both p-type and n-type conducting materials in thermoelectric energy conversion is advantageous due to the Peltier effect and both p and n type conductivities can be found amongst the cuprate high temperature superconductors. In the present study, $Nd_{2-x}Ce_xCuO_4$, which has n-type semiconducting behaviour at low doping levels, was investigated. This superconducting material has electron charge carriers and a superconducting transition temperature, T_c, of $\sim$24 K for an oxygen-deficient $x=0.15$ sample [4]. The literature contains reports on the Seebeck coefficient and electrical resistivity at both low and high temperatures [5–13]. However only a few investigations on the thermal conductivity at elevated temperatures have been reported [14–16].

The purpose of this study is to measure the Seebeck coefficient, electrical resistivity, and thermal conductivity of the title material and to estimate a thermoelectric figure-of-merit and its temperature dependence. The measurements were performed on sintered polycrystalline samples with compositions of $x=0$–0.1 over the temperature range of 300–673 K. The limitations of the power factor, and a possible improvement in the figure-of-merit by a reduction in the thermal conductivity are discussed.

* On leave from Research Development Corporation of Japan, Hon-cho, Kawaguchi, Saitama 332, Japan.

0022–2461

2. Experimental procedures

Sintered discs of $Nd_{2-x}Ce_xCuO_4$ ($x = 0$–0.15) were prepared via a conventional solid state reaction. Reagent grade Nd_2O_3, CeO_2, and CuO powders were thoroughly mixed in a mortar with ethanol being used as a dispersing liquid. The powder mixture was dried and pressed into a pellet which was calcined at 1223 K for 10 h in air. After this calcination step the sample was reground, reformed into a pellet, and reheated. This treatment cycle was repeated a further time and, the produced powder was cold pressed at 200 MPa using a cold isostatic press. The moulded disc was placed onto a Pt sheet and sintered at 1423 K for 12 h in air.

Powder X-ray diffraction patterns were measured with a Philips APD-1700 diffractometer (CuK_α radiation). The a and c lattice constants of the tetragonal Nd_2CuO_4 structure were calculated from the values of the diffraction angles of the $(0\,0\,\underline{1}\,\underline{0})$ and $(2\,0\,8)$ diffraction peaks with Si being used as an internal standard. The composition of the sintered bodies were determined by inductively-coupled-plasma (ICP) emission analysis. The densities of the sintered discs were measured using the Archimedes' method.

Rectangular samples (typically $\sim 5 \times 5 \times 10\ mm^3$) for the electrical measurements were cut from the sintered pellets. Pt wires and two Pt–Pt/13%Rh thermocouples (R–TC) were fixed to the samples using Pt paste (Tanaka Kikinzoku International TR-7905) and the sample was heated at 1173 K for 1 h in air in order to make good electrical and thermal contacts. The electrical resistivity and Seebeck coefficient were measured at several constant temperatures between 300–673 K in air. The electrical resistivity was measured using the d.c. four-probe method. The temperature difference (ΔT) and the thermoelectromotive force (ΔV) between the ends of the samples were measured using two thermocouples and two Pt wires, respectively. By controlling the flow rate of the air, that was blown onto one side of a sample, ΔT could be steadily changed by up to 10 K. The Seebeck coefficient was calculated from the linear gradient of $\Delta V/\Delta T$, and this value was corrected for the absolute thermopower of platinum [19].

The thermal diffusivity and specific heat were measured at several constant temperatures between 300–673 K at ~ 0.1 Pa using laser flash equipment (Sinku-Riko TC-3000). A pulsed ruby laser (energy density : 40 J cm^{-2} wavelength : 694.3 nm, emission time : 800 μs) was used as the light source. An InSb infrared detector was used at 77 K for the thermal diffusivity measurements.

The sintered discs for measurements were polished to a thickness of 0.9–1.0 mm, so that finite pulse-width effects could be neglected (less than 1%). The measured thermal diffusivity data were corrected for heat loss effects using the method of Heckman [20]. Before the specific heat measurements were performed the thermocouples were fixed onto the polished sample surface with Pt paste and the samples were heated at 1173 K for 1 h in air. The maximum temperature rise in a sample produced by a laser flash was calculated from a temperature loss curve obtained by monitoring the rear-surface temperature using the thermocouples. A sapphire was used as a standard in the specific heat measurements. The thermal conductivity was estimated as a product of the density, thermal diffusivity, and specific heat measured on a sample.

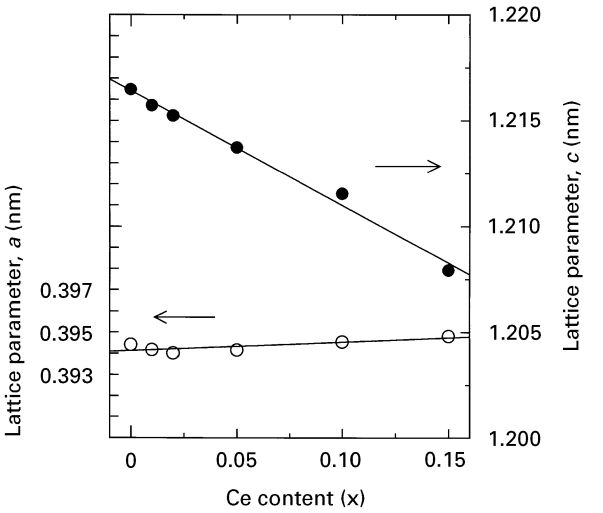

Figure 1 Ce concentration dependences of the a and c lattice constants of the tetragonal Nd_2CuO_4 structure. The lattice parameters were calculated from the diffraction angle values for the $(0\,0\,\underline{1}\,\underline{0})$ and $(2\,0\,8)$ diffraction peaks. Si was used as an internal standard.

TABLE I Atomic ratios of $Nd_{2-x}Ce_xCuO_4$ sintered bodies analysed by ICP. Nd and Ce contents were normalized to corresponding Cu content

X	Nd : Ce : Cu
0	2.15 : – : 1
0.01	2.09 : 0.01 : 1
0.02	2.09 : 0.02 : 1
0.05	2.02 : 0.05 : 1
0.10	1.93 : 0.10 : 1
0.15	1.89 : 0.15 : 1

3. Results

3.1. Identification of sintered samples

Powder X-ray diffraction patterns showed that the $Nd_{2-x}Ce_xCuO_4$ ($x = 0$–0.15) sintered bodies all contained a single phase material that passed the tetragonal Nd_2CuO_4 structure. The variation of the a and c lattice constants as a function of Ce content are shown in Fig. 1. The measured a and c values and their dependence on the Ce content closely agreed with previously reported data [21–23]. The a lattice constant slightly increased with an increase in the Ce concentration whereas the value c significantly decreased. The composition (atomic ratios) of the sintered bodies ($x = 0$–0.15) are listed in Table I in which the analysed Nd and Ce contents are normalized to the corresponding Cu content. The analysed Ce concentrations all agree with the weighted Ce concentrations x. The Nd concentrations were relatively larger than those expected from the stoichiometric ratios, although the difference between the two values decreased with increasing Ce concentration. Thus, the continuous solid solution of Ce atoms into the

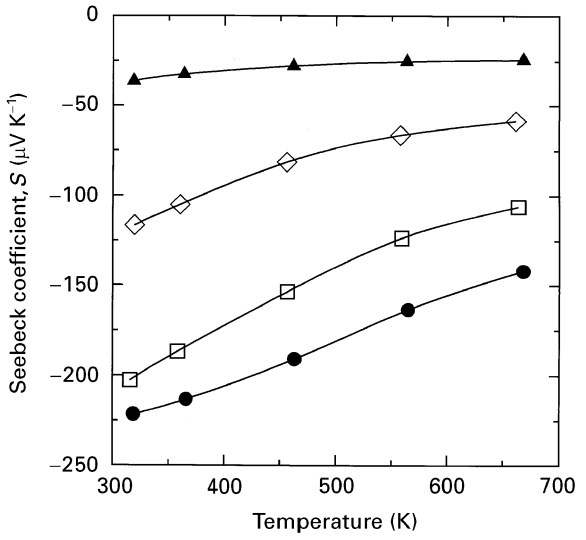

Figure 2 Temperature dependence of the Seebeck coefficient for $Nd_{2-x}Ce_xCuO_4$ ($x =$ (●) 0, (□) 0.01, (◇) 0.05 and (▲) 0.1) sintered bodies. The thermopower values were corrected to allow for the absolute thermopower of platinum [19].

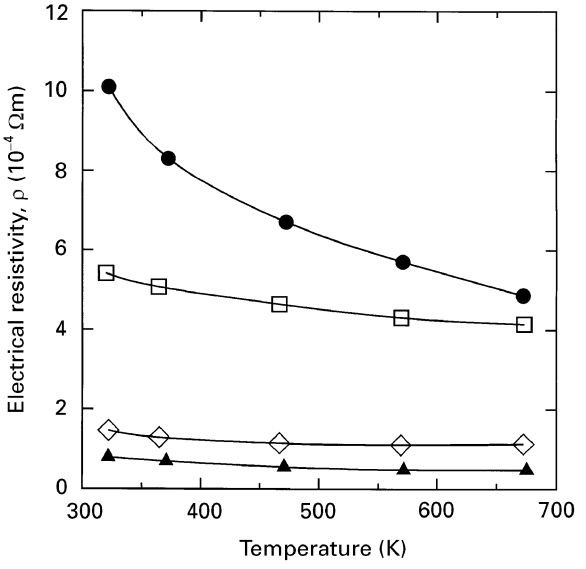

Figure 3 Temperature dependence of the electrical resistivity for $Nd_{2-x}Ce_xCuO_4$ ($x =$ (●) 0, (□) 0.01, (◇) 0.05 and (▲) 0.1) sintered bodies.

Nd_2CuO_4 lattice was confirmed up to $x = 0.15$ in the present samples. The measured densities of the sintered discs were all higher than 95% of the theoretical value.

3.2. Electrical properties and thermoelectric power factor

Figs 2 and 3 respectively show the temperature dependences of the Seebeck coefficient and electrical resistivity of the samples with $x = 0$, 0.01, 0.05, and 0.1. The data were highly reproducible over the measured temperature range. The signs of the Seebeck coefficients were negative for all the measured samples, indicating n-type conduction. The observed negative value for samples with $x = 0$ can be attributed to carrier electrons generated from oxygen vacancies formed during the annealing steps

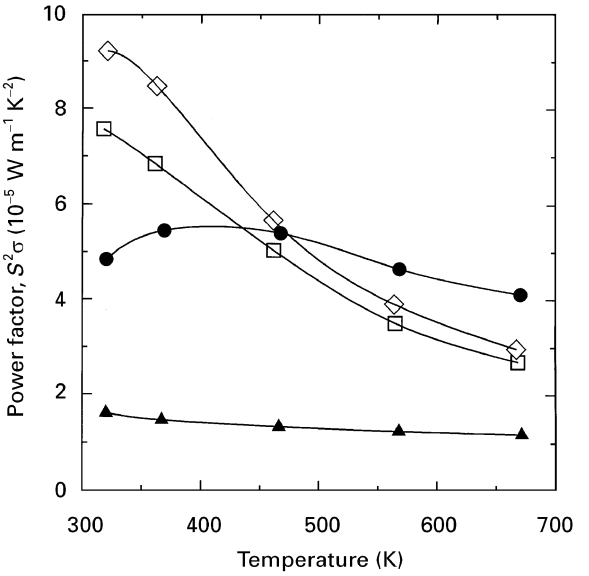

Figure 4 Temperature dependence of the power factor ($S^2\sigma$) estimated from the measured Seebeck coefficient and electrical conductivity data. Key: (●) $x = 0.00$, (□) $x = 0.01$, (◇) $x = 0.05$ and (▲) $x = 0.10$.

[22, 24–28]. The absolute values of the Seebeck coefficient, which were around 100–200 $\mu V K^{-1}$ at room temperature for all samples except for $x = 0.1$, decreased with increasing measurement temperature for all the samples, indicating semiconducting behaviour. The observed temperature dependences closely agree with those previously reported for this material [9, 10]. The temperature dependence of the electrical resistivities of all the measured samples also showed semiconducting behaviour over the measured temperature range. A change to metallic behaviour at slightly higher temperatures has been reported in the literature [10]. Systematic changes in the absolute values of both the Seebeck coefficient and electrical resistivity with increasing cerium content, x, indicate a continuous carrier generation as the Ce substitutes on the Nd sites.

Fig. 4 shows the temperature dependence of the power factor ($S^2\sigma$) estimated from the measured Seebeck coefficient and electrical conductivity values. The values of the power factor were all of the order of 10^{-5} $Wm^{-1}K^{-2}$. Despite showing the highest electrical conductivity value, the power factor for the $x = 0.1$ sample was smaller compared to those for the lightly doped samples. This effect can be attributed to a decrease in the absolute value of the Seebeck coefficient due to a larger carrier concentration in this sample. The power factor values for the $x = 0.01$ and 0.05 samples increased as the temperature decreased and they seem to have their maximum values at a temperature lower than room temperature. The maximum value within the measured temperature range was 9.2×10^{-5} $Wm^{-1}K^{-2}$ at 320 K for the $x = 0.05$ sample.

3.3. Thermal conductivity and thermoelectric figure of merit

Fig. 5 shows the temperature dependence of the thermal conductivity which was calculated as the product

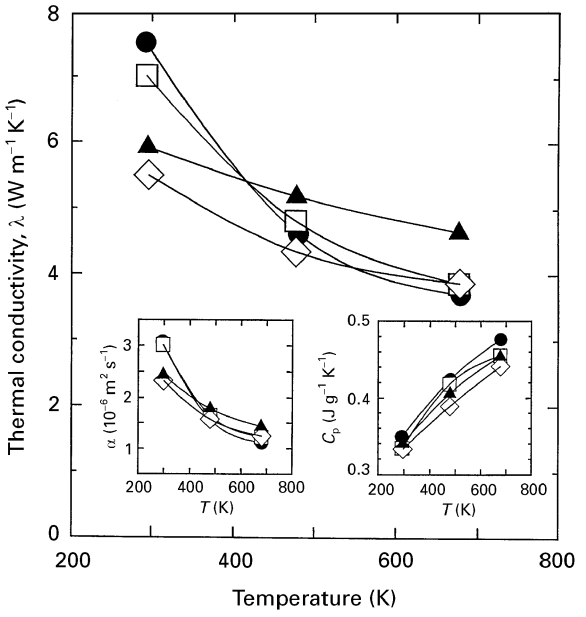

Figure 5 Temperature dependence of thermal conductivity for $Nd_{2-x}Ce_xCuO_4$ (x = (●) 0, (□) 0.01, (◇) 0.05 and (▲) 0.1) sintered bodies. The thermal conductivity was estimated as a product of the density, thermal diffusivity, and specific heat. The density was measured by Archimedes' method. The thermal diffusivity (α) and specific heat (C_p) measured at ~0.1 Pa using the laser flash method are shown in the insets of the figure. A sapphire was used as a standard in the specific heat, measurements.

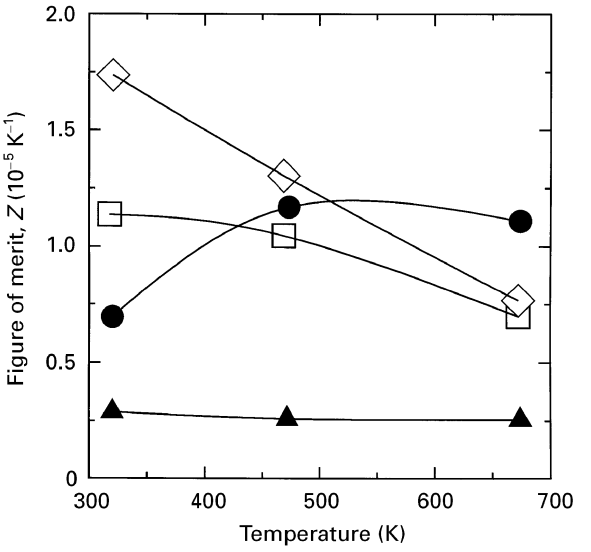

Figure 6 Temperature dependence of the figure-of-merit ($S^2\sigma/\lambda$) estimated from the measured data. Key: (●) $x = 0.00$, (□) $x = 0.01$, (◇) $x = 0.05$ and (▲) $x = 0.10$.

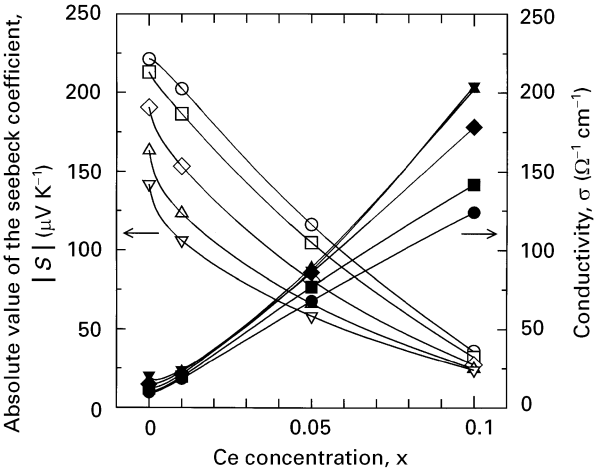

Figure 7 Ce concentration dependences of the absolute values of the Seebeck coefficient ($|S|$) and electrical conductivity (σ) at constant temperatures of: (○, ●) 320 K, (□, ■) 365 K, (◇, ◆) 464 K, (△, ▲) 566 K and (▽, ▼) 669 K.

of the density, thermal diffusivity, and specific heat of a sample. The values of the latter two factors are shown in the insets and they are in reasonable agreement with previously reported data [18]. The absolute values of the thermal conductivities decreased with an increasing temperature for all the investigated samples, and their temperature gradients apparently decreased with increasing cerum content, x. This may be attributed to a decrease in thermal conductivity at lower temperatures, in this case observed at room temperature, due to an increase in the phonon–impurity scattering with increasing cerium content.

The calculated values of the figure-of-merit are shown in Fig. 6. They were all around $1 \times 10^{-5}\,K^{-1}$ except for the $x = 0.1$ sample. The values for the $x = 0.01$ and 0.05 samples appear to have their maximum values at a temperature lower than room temperature, which mimics the behaviour of the power factor. The maximum value obtained over the measured temperature range was $1.7 \times 10^{-5}\,K^{-1}$ at 320 K for the $x = 0.05$ sample.

4. Discussion

We first discuss the electrical properties of the investigated samples and their effect on the power factor. The maximum value of the power factor measured in this study ($9.2 \times 10^{-5}\,W m^{-1} K^{-2}$ at 320 K for the $x = 0.05$ sample) is two orders of magnitude smaller than that of Bi_2Te_3-based samples [29, 30]. This can be attributed to an intrinsically small value of the power factor ($S^2\sigma$) of this material. The Seebeck coefficient and electrical conductivity which determine the power factor are connected with the carrier concentration. As is shown in Fig. 7, the absolute values of the Seebeck coefficient decreased with increasing Ce concentration whereas the electrical conductivities increased. Therefore, we propose that the Ce concentration almost corresponds to the carrier concentration. The relationship between the Seebeck coefficient and electrical conductivity can be understood by eliminating carrier concentration as will now be discussed.

Plots of the Seebeck coefficient (S) against reciprocal temperature gave almost straight lines over the measured temperature range, indicating semiconducting behaviour. It is currently not clear if observed slight differences between the sample $x = 0$ and the other samples is due to Ce-doping. The proportional relationship between S and $1/T$ is given by the following equation:

$$S = -\Delta E/eT + A \qquad (2)$$

where ΔE, e, and A are the carrier generation energy, the electronic charge, and a constant, respectively. ΔE can be expressed as:

$$n = N\exp(-\Delta E/kT) \quad (3)$$

where n, N, and k are the carrier concentration, the density of states, and the Boltzmann constant, respectively. Therefore, the Seebeck coefficient can be expressed as a function of the carrier concentration by:

$$S = -(k/e)(\ln(N/n) + A') \quad (4)$$

Equation 4 has been applied to the case of wide band semiconductors [31, 32] and it can be phenomenologically applied in our case as can be conjectured from Fig. 7. As can also be clearly seen in Fig. 7, on the other hand, the electrical conductivity is expressed by:

$$\sigma = ne\mu \quad (5)$$

where μ is the carrier mobility. From Equations 4 and 5, Jonker's equation [33] which expresses the relationship between the Seebeck coefficient and the electrical conductivity is given by:

$$S = (k/e)(\ln\sigma - \ln(Ne\mu) - A') \quad (6)$$

A positive gradient for a plot of S against $\ln\sigma$, that is $+(k/e)$, is expected in the case where the carriers are electrons. If the product of $N\mu$ remains constant against carrier doping, Equation 6 gives a straight line with a gradient of k/e, and the intercept with $S = 0$ is a constant value for the material.

Mason [3] and Su *et al.* [34] have indicated that a Jonker plot using Seebeck coefficient and electrical conductivity data measured at a high temperature (1043 K) on samples with cerium contents of $x = 0$–0.15 of this material gives a smaller intercept ($\ln\sigma = 5.15\,\Omega^{-1}\,cm^{-1}$) than that ($\ln\sigma = 12.9\,\Omega^{-1}\,cm^{-1}$) of a wide band semiconductor such as the Bi_2Te_3-based material and therefore, the power factor of this material is smaller. Fig. 8 shows a Jonker plot obtained from the present data. As indicated by the dashed line with a gradient of k/e, a good linear relationship was observed for the measured data. The intercept with the axis at $S = 0$ gave a value of $\ln\sigma = 5.13$, which is very close to that given by Su *et al.* [34]. This agreement supports the concept that the intercept at $S = 0$ is a temperature-independent value within this temperature range (320–1043 K). The small value of the intercept may be due to a low mobility in this material as pointed out by Mason [3]. Although a change in the number of in-gap states produced by doping, as is seen in the change of conduction behaviour from insulating to metallic, may bring about a shift of the product $N\mu$, it is probably only observed in the highly doped region beyond $x = 0.15$ as observed in other superconducting materials [35, 36].

The maximum value of the figure-of-merit in this study ($1.7\times10^{-5}\,K^{-1}$ at 320 K for the $x = 0.05$ sample) was also smaller by two orders of magnitude than that of the Bi_2Te_3-based material ($\sim3\times10^{-3}\,K^{-1}$ at 300 K) [29, 30]. As previously described, since the power factor of this material is intrinsically small, a decrease in the thermal conductivity is highly important in any improvement of the figure-of-merit.

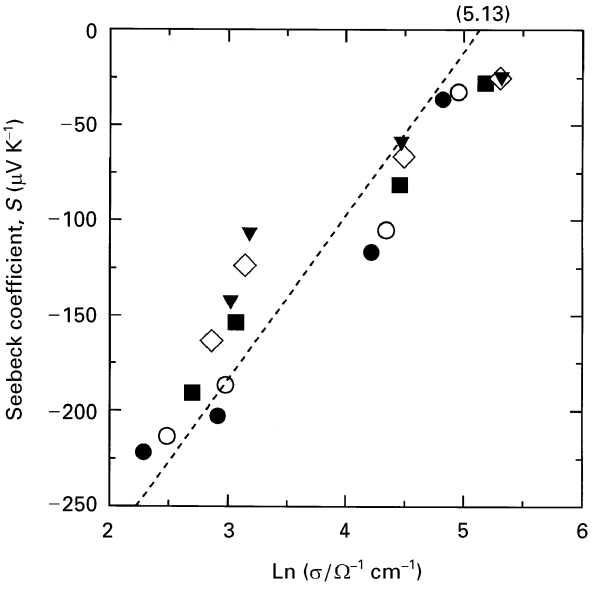

Figure 8 The Seebeck coefficient as a function of the natural logarithm of the electrical conductivity (a Jonker plot). The dashed straight line was determined by a least squares fitting so as to have a gradient of $+(k/e) = 86.17\,\mu V\,K^{-1}$. The intercept at $S = 0$ gave a value of $\ln\sigma = 5.13$. Key: (●) 320 K, (○) 365 K, (■) 464 K, (◇) 566 K and (▼) 669 K.

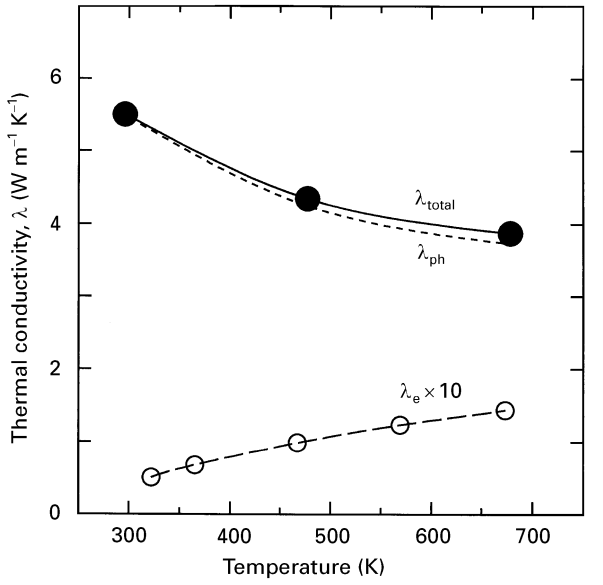

Figure 9 Temperature dependences of the total (λ), electron (λ_e), and phonon (λ_{ph}) thermal conductivities for the $x = 0.05$ sample. The electron thermal conductivity was estimated from the electrical conductivity data by use of the Wiedemann–Franz law.

The temperature dependence of the thermal conductivity for the $x = 0.05$ sample is again presented as Fig. 9. The measured thermal conductivity was separated into electron and phonon components by $\lambda = \lambda_e + \lambda_{ph}$, where λ, λ_e, and λ_{ph} are the total, electron, and phonon thermal conductivities, respectively. By applying the Wiedemann–Franz law to the electrical conductivity data, the electron thermal conductivity could be estimated as $\lambda_e = L\sigma T$, where L is the Lorenz number, $2.44\times10^{-8}\,V^2\,K^{-2}$ [37]. As is shown in Fig. 9, although the electron thermal conductivity increased with an increase in the temperature, it remains small compared with the total thermal

conductivity. Most of the total thermal conductivity was composed of the phonon component as indicated by the dashed line in Fig. 9. This is in agreement with the observed decrease in the thermal conductivity at lower temperatures with increasing Ce concentration. The large phonon component conversely indicates that the electrical conductivity is small at the optimum Ce concentration due to an intrinsically small $S^2\sigma$. For such materials, an improvement in the figure-of-merit can be attempted to some extent by controlling the sample texture, which is expected to decrease the phonon thermal conductivity.

5. Conclusions

Values of the thermoelectric power factor and figure-of-merit for $Nd_{2-x}Ce_xCuO_4$ ($x = 0$–0.1) sintered bodies were estimated from values of the Seebeck coefficient, electrical resistivity, and thermal conductivity measured in the temperature range of 300–673 K. The temperature dependences of both the Seebeck coefficient and electrical resistivity indicated n-type semiconducting behaviour. The thermal conductivities, that decreased with increasing temperature, were in the range of 3.7–7.5 $Wm^{-1}K^{-1}$. The maxima of the power factor and figure-of-merit in this study for a sample of composition $x = 0.05$ were estimated to be 9.2×10^{-5} $Wm^{-1}K^{-2}$ and 1.7×10^{-5} K^{-1} respectively, at 320 K. The maxima of this sample appears to be located at temperatures lower than room temperature. The thermal conductivity was separated into a small electron component and a large phonon component by applying the Wiedemann–Franz law. A certain improvement in the figure-of-merit could be achieved by a reduction in the phonon thermal conductivity.

Acknowledgements

The authors would like to acknowledge Professor K. Koumoto, Dr W. S. Seo, and Mr H. Ohta of Nagoya University for advice on the transport property measurements and Dr A. Tsuge for the ICP emission analysis. One of the authors (M. Y.) wishes to acknowledge Professor H. Kawazoe of Tokyo Institute of Technology for improving the manuscript.

References

1. S. UCHIDA, H. TAKAGI and Y. TOKURA, *Physica C* **162–164** (1989) 1677.
2. W. J. MACKLIN and P. T. MOSELEY, *Mater. Sci. Engng* **B7** (1990) 111.
3. T. O. MASON, *ibid.* **B10** (1991) 257.
4. Y. TOKURA, H. TAKAGI and S. UCHIDA, *Nature* **337** (1989) 345.
5. S. UJI, H. AOKI and T. MATSUMOTO, *Jpn J. Appl. Phys.* **28** (1989) L563.
6. M. E. LOPEZ-MORALES, R. J. SAVOY and P. M. GRANT, *Solid State Commun.* **71** (1989) 1079.
7. Z. S. LIM, K. H. HAN, S.-I. LEE, Y. H. JEONG, S. H. SALK, Y. S. SONG and Y. W. PARK, *Phys. Rev. B* **40** (1989) 7310.
8. V. VIJAYASHREE, C. K. SUBRAMANIAM and R. SRINIVASAN, *Bull. Mater. Sci.* **14** (1991) 831.
9. T. OHTANI, K. KOBATAKE and T. TAKEHARA, *Physica C* **179** (1991) 376.
10. J. TAKEDA, T. NISHIKAWA and M. SATO, *ibid.* **231** (1994) 293.
11. S. J. HAGEN, X. XU, J. L. PENG, Z. Y. LI, W. JIANG and R. L. GREENE, *ibid.* **185–189** (1991) 1275.
12. *Idem*, *Phys. Rev. B* **45** (1992) 515.
13. F. MUNAKATA, T. KAWANO, A. NOZAKI and H. YAMAUCHI, *J. Appl. Phys.* **67** (1990) 4159.
14. M. VLCEK, L. BENES and J. HORAK, *Czech. J. Phys.* **40** (1990) 1057.
15. M. VLCEK and L. BENES, *ibid.* **43** (1993) 575.
16. J. L. COHN, M. S. OSOFSKY, J. L. PENG, Z. Y. LI and R. L. GREENE, *Phys. Rev. B.* **46** (1992) 12053.
17. A. JEZOWSKI and P. W. KLAMUT, *J. Less-Common Metals* **169** (1991) L17.
18. E. TAKEGOSHI, Y. HIRASAWA, T. SHIMAZAKI and K. OKUI, *Netsu Bussei* **7** (1993) 82.
19. N. CUSACK and P. KENDALL, *Proc. Phys. Soc. London* **72** (1958) 898.
20. R. C. HECKMANN, *J. Appl. Phys.* **44** (1973) 1455.
21. H. TAKAGI, S. UCHIDA and Y. TOKURA, *Phys. Rev. Lett.* **62** (1989) 1197.
22. F. IZUMI, Y. MATSUI, H. TAKAGI, S. UCHIDA, Y. TOKURA and H. ASANO, *Physica C* **158** (1989) 433.
23. P. H. HOR, Y. Y. XUE, Y. Y. SUN, Y. C. TAO, Z. J. HUANG, W. RABALAIS and C. W. CHU, *ibid.* **159** (1989) 629.
24. J. S. KIM and D. R. GASKELL, *ibid.* **209** (1993) 381.
25. M. SCAVINI, G. CHIODELLI, G. SPINOLO and G. FLOR, *ibid.* **230** (1994) 412.
26. H. ISHIZUKA, Y. IDEMOTO and K. FUEKI, *ibid.* **209** (1993) 491.
27. Y. IDEMOTO, K. FUEKI and T. SHINBO, *ibid.* **166** (1990) 513.
28. S. YAMAGUCHI, K. YASUI, F. MATSUMOTO, K. TERABE, T. SUKIGARA and Y. IGUCHI, *Solid State Ionics* **49** (1991) 63.
29. W. M. YIM, E. V. FITZKE and F. D. ROSI, *J. Mater. Sci.* **1** (1966) 52.
30. W. M. YIM and F. D. ROSI, *Solid State Electr.* **15** (1972) 1121.
31. I. G. AUSTIN and N. F. MOTT, *Adv. Phys.* **18** (1969) 41.
32. H. FRITZSCHE, *Solid State Commun.* **9** (1971) 1813.
33. G. H. JONKER, *Phil. Res. Rep.* **23** (1968) 131.
34. M.-Y. SU, C. E. ELSBERND and T. O. MASON, *Physica C* **160** (1989) 114.
35. *Idem.*, *J. Amer. Ceram. Soc.* **73** (1990) 415.
36. M.-Y. SU, E. A. COOPER, C. E. ELSBERND and T. O. MASON, *ibid.* **73** (1990) 3453.
37. M. E. FINE and N. HSIEH, *ibid.* **57** (1974) 502.

Received 19 August 1996
and accepted 22 May 1997